International Journal of Engineering Trends and Technology
ISSN: 2231–5381 / https://doi.org/10.14445/22315381/IJETT-V71I6P220

Volume 71 Issue 6, 181-195, June 2023

Original Article

Design and Modelling of Analysis of Kerwin, Huelsman, and Newcomb (KHN) Biquad Filter using Double-Gate MOSFET for Low Energy Devices

Zethembe S. Madonsela[1], Viranjay M. Srivastava[2]

[1,2]*Department of Electronic Engineering, Howard College, University of KwaZulu-Natal, Durban, South Africa*

[2]*Corresponding Author : viranjay@ieee.org*

Received: 08 March 2023 Revised: 05 May 2023 Accepted: 19 June 2023 Published: 25 June 2023

Abstract *- This work designs a Kerwin, Huelsman, and Newcomb (KHN) biquad filter using Double-Gate (DG) MOSFETs. The differential amplifier topology has been used to realize and analyze this device to conserve energy. The KHN Biquad filter prototype has been fabricated and verified. Various parameters such as the center frequency, DC gain, bandwidth, power dissipation, and quality issue have been discussed. The sub-sections of this device, such as the high-pass stage filter, pass frequencies above 10 kHz; the band-pass stage filter works well for frequencies range 4 kHz - 45 kHz, and the low-pass filter allows frequencies less than 10 kHz. This device provides a Universal Biquadratic filter that dissipates less power than the original KHN biquad filter.*

Keywords *- Double-gate MOSFET, KHN Filter, Differential amplifier, Low energy device, Microelectronics, VLSI.*

1. Introduction

Filters can separate signals, allowing only the relevant frequencies to pass while attenuating the undesired ones. Filters are also employed in data conversion to remove the effects of aliases in analog and digital systems [1-3]. They are also used to smooth the waveform at the output of a digital or analog system by reconstructing the signal and removing higher frequency components like the sampling frequency and its harmonics [4]. In high-gain amplifiers or single supply circuits, DC offset can be stopped using a straightforward single-pole high-pass filter [5]. An example of a multiple-feedback filter circuit is the Kerwin, Huelsman, and Newcomb (KHN) filter, which may simultaneously provide the filter responses such as Low Pass (LP), High Pass (HP), and Band Pass (BP) from a single active filter design. These transfer functions are realized via biquadratic (Biquad) circuits [6, 7].

The KHN biquad is similar to the state variable filter and can be designed using various techniques [8]. The transfer function is quadratic in the numerator, and the denominator, hence the name; A biquadratic function is the transfer function as a result. Looking at the previously designed KHN filter circuits were designed using numerous methods, but most are op-amps [9, 10]. Ibrahim et al. [11] have realized that gain-bandwidth amplifier operating products do not affect current conveyors. Naidoo et al. [12] have suggested that the operational amplifiers and single-gate MOSFETs are examples of conventional components with higher power requirements and larger electronic package sizes. The voltage-mode KHN biquad filter has more power consumption and less bandwidth than the current-mode counterpart [13]. The current-mode KHN biquad filter using modified CFTAs, frequency, and quality factor (Q) cannot be independently tuneable. The frequency for the biquad filter can be tuned from 8.16 kHz to 628 kHz, and the minimum phase noise in the entire tuning range is 90.3 dB/Hz with an offset frequency of 100 Hz [14, 15]. A KHN filter circuit suggested by Koksal and Sagbas [16] relies on several resistors to switch from the current mode to the voltage mode and is not electronically adjustable. Bekri and Anday [17] have suggested a current differencing transconductance amplifier. However, the filter can only be designed as a low-pass, and the properties of the transfer function cannot be achieved. The suggested RC-RC decomposition current-mode filter had the drawback of requiring numerous passive parts in its construction. A square root domain lossless integrator KHN biquad filter was proposed by Olmez and Cam [18]. The MOS transistor was used to create the biquad filter. The secondary effects result in variations from the ideal MOS transistor properties because the MOS transistor's dimensions are shrinking.

Hamid and Colombo [19] provided a fully simulation-based approach to designing analog circuits in 2008. In the optimization process, yield is used as the cost function. It was

based on the non-overlapping population GA technique. Based on the population size, the algorithm creates a random initial generation of individuals and then creates new sets of individuals with each subsequent generation. The concepts had been put into practice employing 0.35-m AMS technology on balanced OTA. Hamed et al. [20] investigated the fractional-order KHN low-pass and high-pass filters based on four approximation techniques: continued fraction expansion, matsuda, oustaloup, and valsa. Fractional-order filter fundamentals were reviewed afterwards; a comparison was made between the ideal and actual characteristics of the filter, realized with each approximation. The operational amplifier becomes heats up whenever used for a long time. Hence more power will be consumed (according to Ohm's law) [48].

The proposed design solution is to improve the KHN filter's performance regarding power consumption, accuracy, efficiency, noise, and reducing thermal effect. The outputs of the KHN filter simultaneously include low-pass, high-pass, and band-pass filters. The voltage-mode KHN filter presented has an electrically tuned cut-OFF frequency and quality factor. The proposed filter circuit is designed and analyzed to enhance the linearity and other properties of the KHN biquad filter. This work will analyze the parameters: frequency, Q-factor, voltage, and current mode. The DG MOSFETs have been used as a possible design solution to encounter the setbacks KHN filters face (using op-amp). Modern amplifiers have a flat frequency response of 425 kHz. The designed version of KHN biquad uses a differential DG MOSFETs amplifier to reduce noise and power consumption. This paper has been organized as follows. Section 2 has the design methodology for this device. Section 3 discusses the op-amp-based KHN; however, Section 4 has the design and analysis of the DG MOSFET-based KHN biquad filter. Section 5 has a prototype design and analysis of this DG MOSFET-based KHN biquad filter. Finally, Section 6 concludes the work and recommends future aspects.

2. Design Methodology

The DG MOSFETs are good alternatives since they enhance the device's performance features while having a compact architecture. Figure 1 illustrates the process of designing the KHN biquad filter using DG MOSFET [22-24]. The KHN biquad filter simultaneously produces high-pass, band-pass, and low-pass responses. Separate tests have been performed on the filter stages to ensure they produce the desired frequency response. The filtered outputs have been viewed with a spectrum analyzer. The high-pass stage filter will pass frequencies above 10 kHz, the band-pass stage filter will pass frequencies that range between 4 kHz- 45 kHz, and the low-pass filter will allow frequencies less than 10 kHz to pass.

2.1. Double-Gate (DG) MOSFET

The BF998 Double-Gate (DG) MOSFET has been used for the circuit design because of its low voltage (5 V) supply.

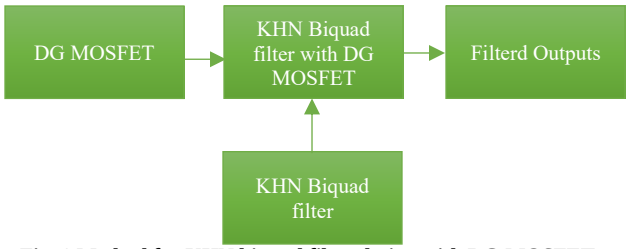

Fig. 1 Method for KHN biquad filter design with DG MOSFET

With a high forward transfer admittance to input capacitance ratio, the DG MOSFET has a high forward transfer admittance and short channel transfer. A low noise gain amplifier for frequencies up to 1 GHz is available in the BF998. With a voltage supply ranging from 3 V to 7 V, the DG MOSFET is appropriate for use in Very High Frequency (VHF) and Ultra-High Frequency (UHF) applications. The BF998 MOSFET needs a positive voltage input to operate as an enhancement-type transistor [25-27]. The DG MOSFET has superior power efficiency and switching capabilities than the single-gate MOSFET because it has a lower width and provides better gate control over the channel. As a result of the DG MOSFET's smaller size, the filter circuit may become smaller, resulting in a reduction in the circuit's overall weight, which reduces the heat generation inside the circuit during its working conditions. Hence the filter circuit will be more efficient. Fig. 2 shows the double-gate MOSFET schematic.

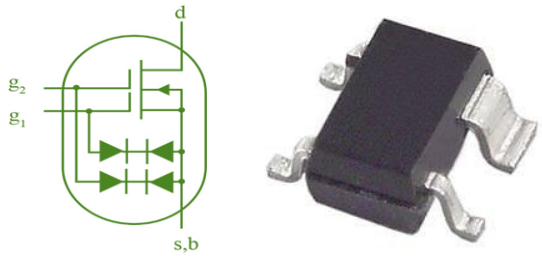

Fig. 2 Basic design of BF998 dual-gate MOSFET

The introduction of DG MOSFET as a bridge to new technologies and a way around single-gate MOSFE's challenges. These MOSFETs have achieved extended scaling below 65-nm technology and have gate lengths as small as 25 nm [3, 23, 24, 27]. The subthreshold swing is inversely proportional to MOSFETs' channel length and threshold voltage, although the two parameters are directly correlated in other devices. As length decreases, the Short Channel Effects (SCEs) are generally induced by lateral electric fields from source to channel and drain to channel [28-30]. Focusing on the design and manufacture of the DG MOSFET, using two gates enables active control of the electric field generated by offering the user more channel control than in single-gate devices. Given that they are common single-gate (SG) MOSFETs like the 2N7000, important parametrization has been considered, such as explicit threshold voltage models incorporating gate-to-source voltages for both gates of the DG MOSFET and their relationship. The maximum operating conditions for the BF998 MOSFET are shown in Table 1.

Table 1. Maximum operating conditions for the BF998 MOSFET

Symbol	Parameter	Max
V_{DS}	Drain-source voltage	12 V
I_D	Drain current	30 mA
P_T	Total power dissipation	200 mW
F	Noise figure (800 MHz)	1 dB

It permits a maximum drain-source voltage of 7 V, a maximum drain current of 30 mA, a maximum total power dissipation of 200 mW, and a noise figure of 2.8 dB at an operating frequency of 800 MHz. The saturation region for the double gate MOSFET starts when the drain-source voltage is 4 V and gate-1 to the source is 0.4 V; the drain current is at maximum (I_d = 21 mA). The drain current in the saturation region can be expressed as [3, 23, 24]:

$$I_{ds} = \mu_{eff} C_{oxeff} \frac{W}{L}\left[(V_{g1} - V_0)^2 - \frac{8rk^2T^2}{q^2} e^{q(V_{g1}-V_0-V_{ds})/kT}\right] \quad (1)$$

where μ_{eff} is the effective mobility and C_{oxeff} is the effective capacitance oxide. V_o is close to the threshold voltage of DG MOSFETs and relates to Silicon thickness. Here, V_o is produced by:

$$V_0 = \frac{2kT}{q} \ln\left[\frac{2}{t_{si}}\sqrt{\frac{2\varepsilon_{si}kT}{q^2 n_i}}\right] \quad (2)$$

Where t_{si} is the Silicon thickness and is proportional to the subthreshold. The drain current in the subthreshold zone can be expressed as [3, 23, 24]:

$$I_{ds} = \mu_{eff} \frac{W}{L} kTn_i t_{si} e^{q(V_{g1})/kT}\left[1 - e^{-q(V_{ds})/kT}\right] \quad (3)$$

The transconductance and the OFF-state current can be estimated using the drain current expression in the saturation area and the subthreshold region [3, 23, 24]:

$$g_m(x) = \frac{dI_{ds}}{dV_{g1}}|_{Vds} = \mu_{eff} C_{oxeff} \frac{W}{L}\left[2(V_{g1} - V_0) - \frac{8rkT}{q} e^{q(V_{g1}-V_0-V_{ds})/kT}\right] \quad (4)$$

For the OFF-state current, V_{ds}=0. Hence, the OFF-state current is expressed as [3, 23, 24]:

$$I_{OFF}(x) = \mu_{eff} \frac{W}{L} kTn_i t_{si}\left[1 - e^{-q(V_{ds})/kT}\right] \quad (5)$$

However, in this work, the operational amplifiers (op-amp) have not been used as a possible solution for the design. The DC gain of the filter circuit is (with op-amp) at -3 dB, which translates to an open loop voltage gain, as seen from the filter's response curves in Fig. 3(b). The response also demonstrates that the Q value causes the output curves to peak at a maximum voltage gain at the corner frequency. The low-pass, high-pass, and band-pass filters were cascaded to produce the output signals in Fig. 3(a). The low-pass, high-pass, and band-pass filter circuits have been realized independently before being cascaded to match the design requirements. The input signal is linked directly to the inverting input terminal of the op-amp, causing integrators to produce a phase lag with a negative sign denoting an 180^0 phase shift. The op-amp (A3's) input signal is connected to the output of the op-amp that comes before it, A2; hence its input is represented as V_{BP} and its output is given as V_{LP} in this instance. Then, using the op-amp basic equation, the transfer function for A3 can be given as [34, 35]:

$$A_3 = \frac{V_{LP}}{V_{BP}} = -\frac{1}{2\pi f_C RC} \quad (6)$$

To find the transfer function for A_2, the same method used to find A_3 will be used. The input voltage is the high pass filter circuit V_{HP} signal.

$$A_2 = \frac{V_{BP}}{V_{HP}} = -\frac{1}{2\pi f_C RC} \quad (7)$$

The output from the first op-amp integrator (V_{BP}) becomes the input of the second since the two op-amp integrators, A_2 and A_3, are cascaded. As a result, the following is the transfer function between V_{HP} and V_{LP}:

$$\frac{V_{LP}}{V_{HP}} = A_2 * A_3 = \frac{1}{(2\pi f_C RC)^2} \quad (8)$$

The two amplifier circuits can be considered one single integrator circuit with a cut-off frequency if the same values for R and C are utilized to ensure that the two circuits have the same integrator time constant. The cut-off frequency [34, 35]:

$$2\pi f_C = \sqrt{\frac{R_3}{R_4(RC)^2}} \quad (9)$$

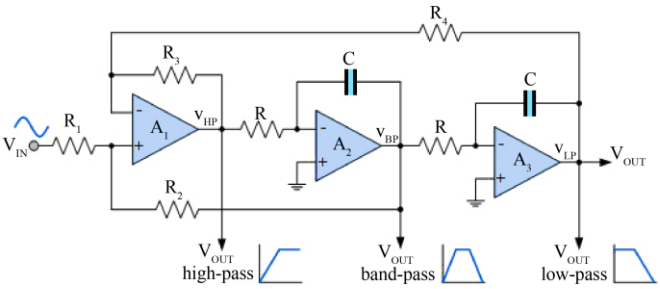

Fig. 3 (a)

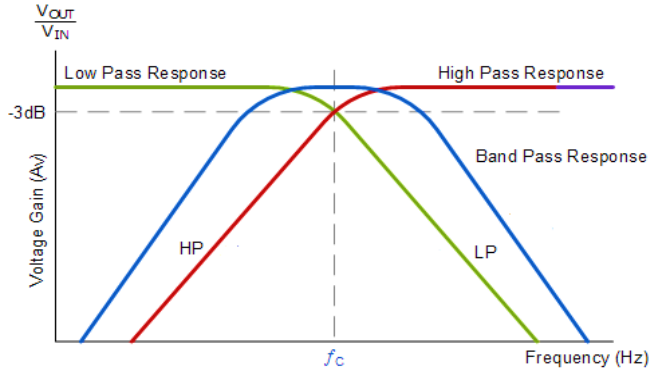

Fig. 3 (b)

If $R_3 = R_4$, then the cut-off frequency becomes:

$$f_C = \frac{1}{2\pi RC} \tag{10}$$

The Q factor for the band-pass filter is [34, 35]:

$$Q = \frac{f_C}{BW} = \frac{R_1(R_3+R_4)}{R_4(R_1+R_2)}\sqrt{\frac{R_3RC}{R_4RC}} \tag{11}$$

If $R_3 = R_4$ and components C and R for both integrators are equal. This implies that the square-root expression is 1. The results from the two integrators, A_2 and A_3, are V_{BP} and V_{LP}, respectively. The transfer function of the biquad filter is obtained by changing the integrator equations for A_2 and A_3 in the preceding equation. Therefore, the transfer function is:

$$T(s) = \frac{V_O}{V_i} = \frac{V_{LP}}{V_{IN}}$$

$$\frac{V_{LP}}{V_{IN}} = \frac{\frac{R_2(R_3+R_4)}{R_3(R_1+R_2)}\times\frac{1}{RC}}{\frac{R_3}{R_4RC}\times\frac{R_1(R_3+R_4)}{R_4(R_1+R_2)}\times\frac{1}{2\pi f_C RC}+\frac{1}{(2\pi f_C RC)^2}} \tag{12}$$

This transfer function resembles the normalized second-order response.

3. Analysis of op-amp-based KHN

The circuit in Fig. 4 has been used as a solution for the KHN biquad filter. This design will be used as a bridge to get the required specification for the following sections. These calculations have been computed to select specific components for the KHN biquad filter based on amplifiers in Fig. 3(a). Since the three signals have the same cut-off frequency. The cut-off frequency is 10 kHz from the specification. By selecting C to be 1 nF, using Eq. (10), R is:

$$R = \frac{1}{2\pi Cf_C} = \frac{1}{2\pi(1\times10^{-6})(10\times10^{3})} = 15915.49\Omega$$

therefore, the resistor R is 15 kΩ. To get the values for R_1 and R_2, Eq. (11) has been used, and the Q-factor is 2. Since $R_3 = R_4$ and both integrators have the same values for R and C, then R_1 and R_2 are:

$$Q = \frac{R_1(R_3+R_4)}{R_4(R_1+R_2)}$$

Selection R_1 = 10 kΩ and $R_3 = R_4$ to 10 kΩ. Hence, R_2 is:

$$R_2 = \frac{R_1(R_3+R_4)}{Q^{-1}R_4} - R_1 = \frac{10k\Omega(10k\Omega+10k\Omega)}{2^{-1}(10k\Omega)} - 10k\Omega = 40k\Omega$$

Therefore, the selected value for R_2 is 30 kΩ. Ao expresses the DC pass-band gain; this gain is sampled from Eq. (12):

$$A_o = \frac{R_2(R_3+R_4)}{R_3(R_1+R_2)} = \frac{30k\Omega(10k\Omega+10k\Omega)}{10k\Omega(10k\Omega+30k\Omega)} = 1.5$$

The gain in terms of decibels is: $A_o = 20\log 1.5 = 3.52dB$. The maximum gain of the filter can be calculated by multiplying A_o and Q-factor: $A_o \times Q = 1.5(2) = 3 = 9.54dB$. The design of the KHN biquad filter is C = 1 nF, R = 15 kΩ, R_1 = 10 kΩ and R_2 =30 kΩ, R_3 = 10 kΩ, and R_4 =10 kΩ as shown in Fig. 4. All the circuits designed in this work are designed using Multisim (v14.1).

After simulating the circuit, the high-pass, band-pass, and low-pass output was displayed using the bode plot. The cut-off frequency for the signals when C is assumed 1 nF and R is calculated to be 15.9 kΩ is 10 kHz. The maximum gain is equivalent to the calculated gain. The output signals are shown in Fig. 5.

After simulating the circuit, it has been proven that op-amp frequencies are limited, as shown in Fig. 5(a) high-pass filter section.

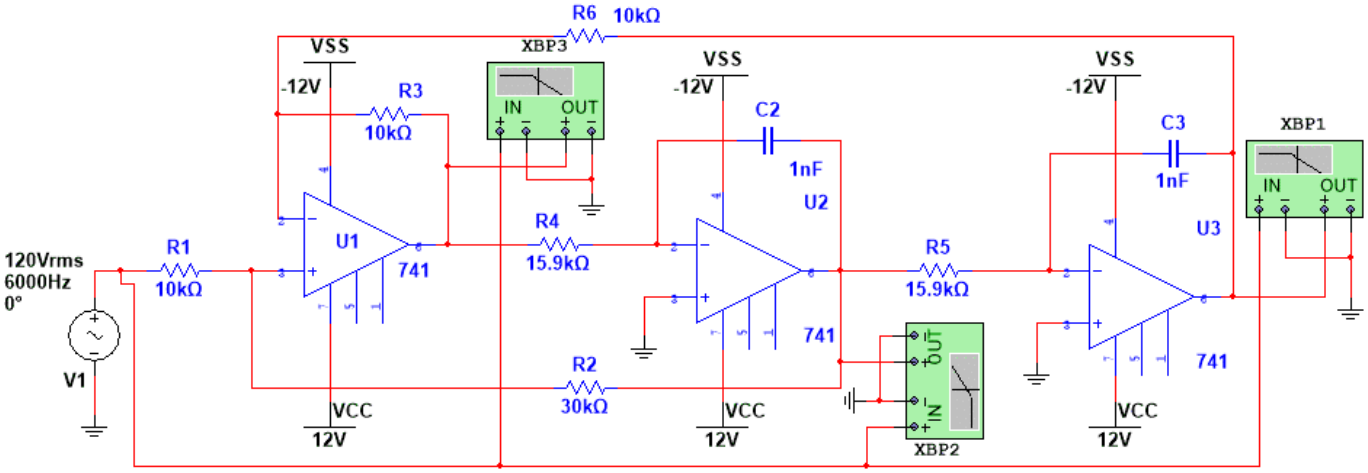

Fig. 4 The KHN biquad filter using op-amps

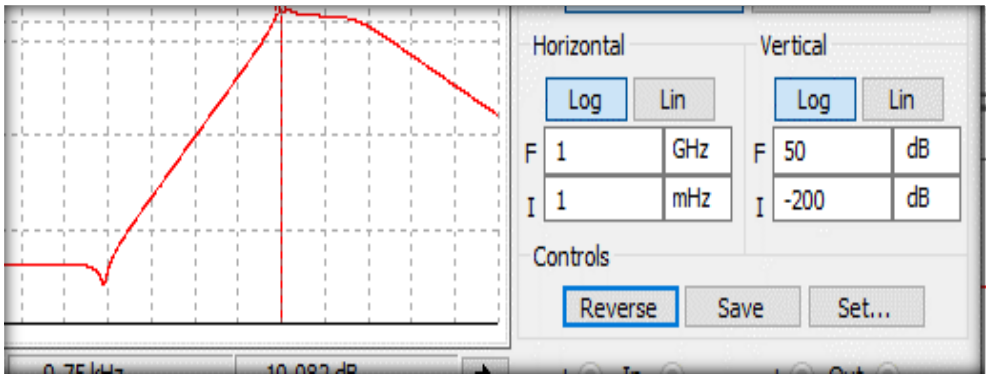

(a)

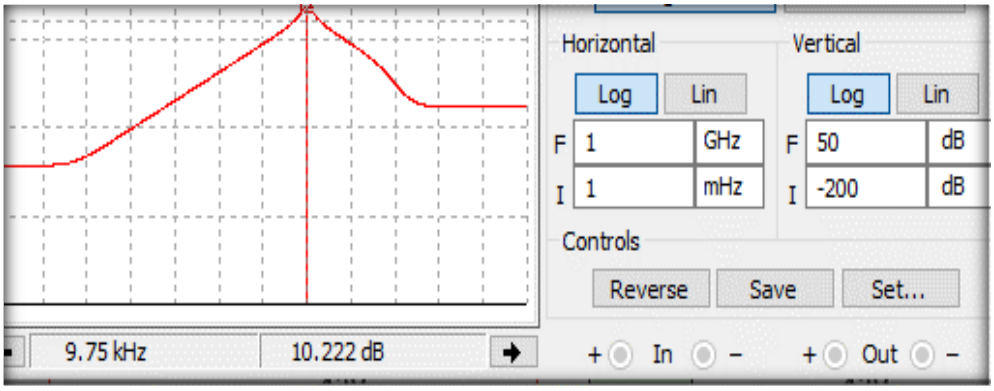

(b)

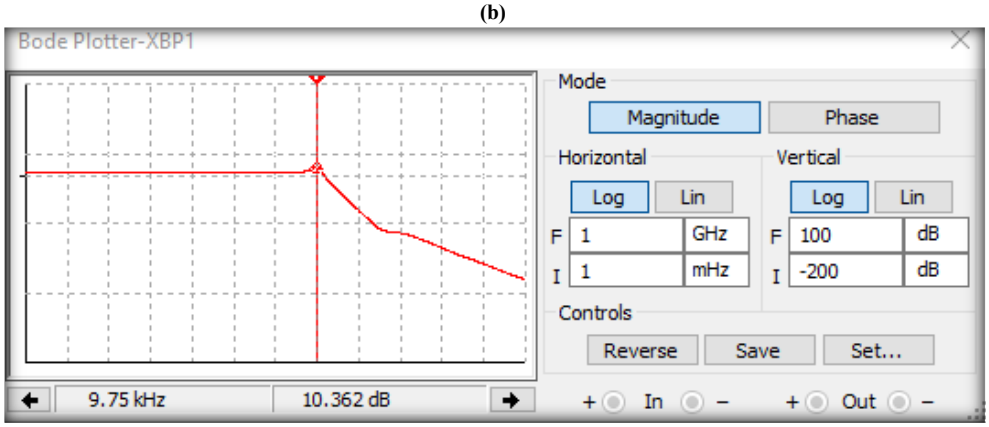

(c)

Fig. 5 (a) High-pass filter signal, (b) band-pass filter signal, and (c) low-pass filter signal

4. Design and Analysis of Double-Gate MOSFET-based KHN

The circuit shown in Fig. 6 is used to replace the three amplifiers [36, 37]. The final designed circuit is shown as the proposed solution in Fig. 7. The differential DG MOSFET operates on the input signal's saturation through gate-1 and gate-2. The DC current in point PR_3 in R_{12} is the sum of the DC current in R_1 and R_2. In ref [8, 28], the amplifiers are converted to double-gate MOSFET, as shown in Fig. 7. The proposed solution uses the BF998 Silicon N-channel double-gate MOSFET, which is shown in Fig. 7. This MOSFET leads to a reduction in the filter circuit's size. It, therefore, reduces the overall weight of the circuit. The performance and reliability of the KHN biquad filter will be improved if the BF998 is used instead of SG MOSFET. The system will be suitable for high-frequency applications since utilizing a DG device reduces the input capacitance. The gate-to-channel coupling is doubled in the BF998 MOSFET, which improves the Short-Channel Effects (SCEs) experienced by SG MOSFETS [38-41]. This research work uses DG MOSFET, such as BF998, as an alternative for simulation.

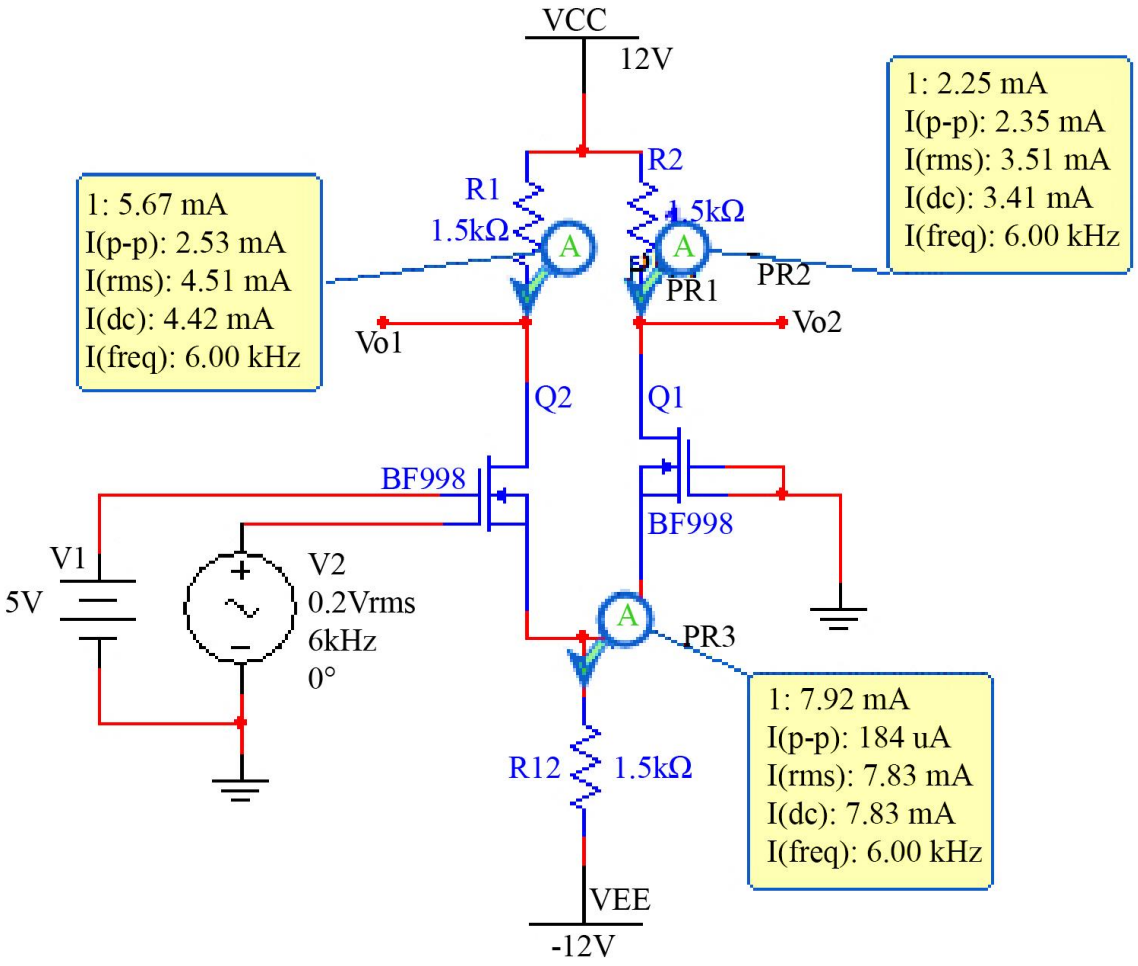

Fig. 6 Double-gate MOSFE T differential amplifier

The KHN biquad filter using DG MOSFETs in Fig. 7 has been analyzed using its small-signal model circuit. The circuit is separated into three segments (high-pass, band pass, and low-pass filter). The biquad filter is a staged circuit with three output signals, and the high-pass filter output signal is the input signal to the band-pass filter. The output signal from the band-pass filter is the input to the low-pass filter. Calculations are made based on the internal structure of the DG MOSFETs.

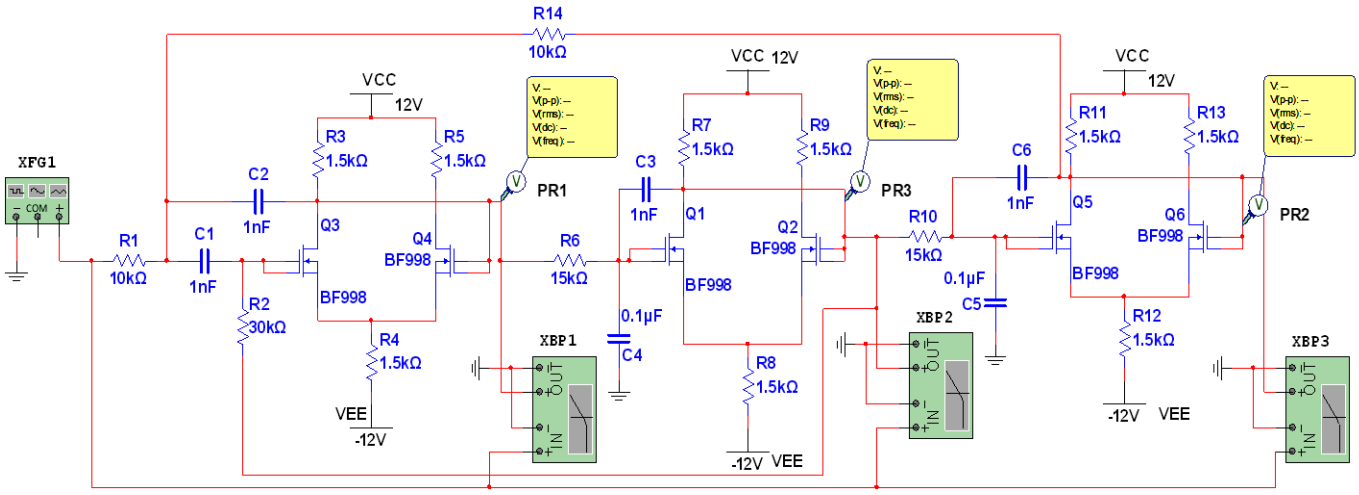

Fig. 7 KHN Biquad filter using BF998

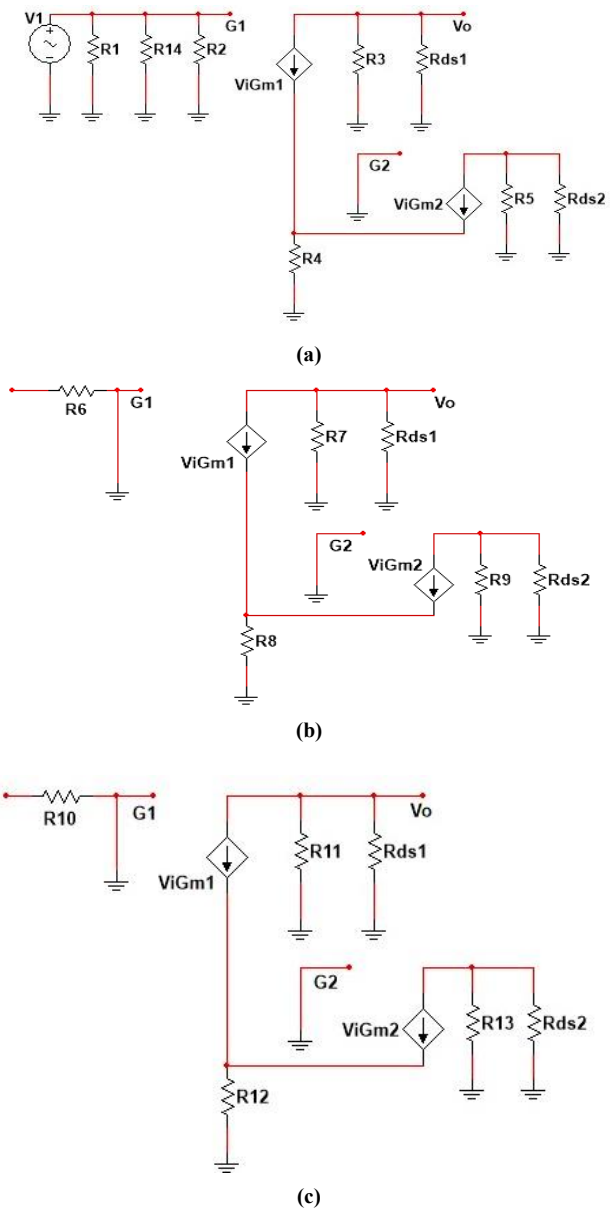

Fig. 8 Small-signal model for (a) high-pass, (b) band-pass, and (c) low-pass filter

To calculate the DC gain for the DG MOSFET small-signal circuit. The input V_1 is the sum of the current flow between R_1 and R_{14}, equivalent to $i=V_iG_{m1}$. Therefore, the input voltage is: $i[R_1||R_{14}||)R_2]$. The output voltage Vo is: $\propto i(R_3||R_{ds})$. The gain for gate-1 is:

$$A_{Vds} = \frac{V_o}{V1} = \frac{\propto i(R_3||R_{ds1})}{i[(R_1||R_{14}||R_2)]} = \frac{\propto (R_3||R_{ds1})}{[(R_1||R_{14}||R_2)]}$$

Since the input voltage for gate-2 is zero, this implies that the DC gain is infinite. A resistor can be added to resolve this so the voltage is not zero. Where R_{ds} is the internal resistance of the MOSFET. From Fig. 8(a), the input voltage is the output from the high-pass filter

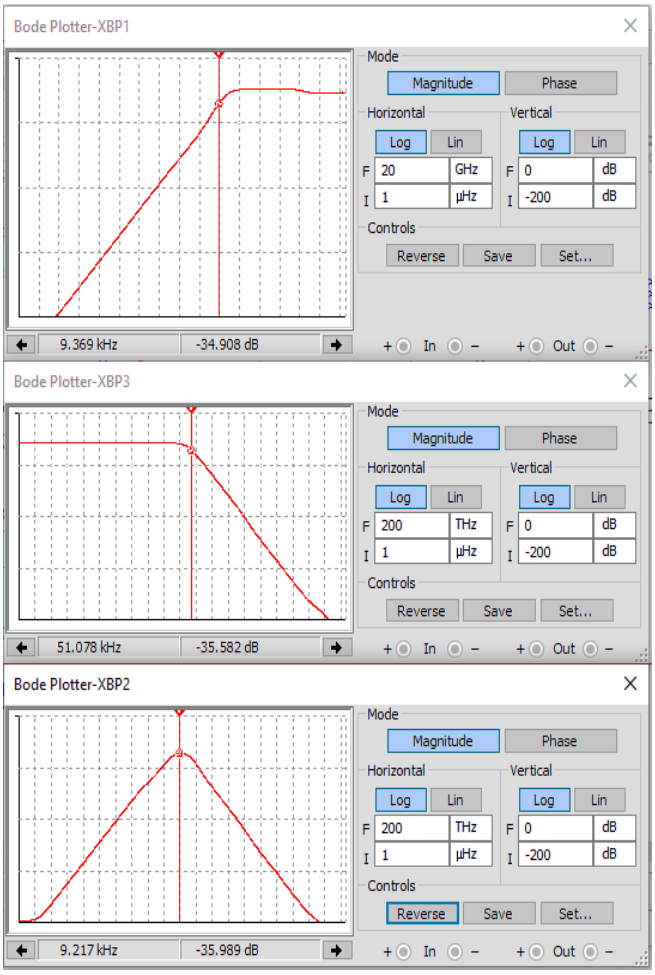

Fig. 9 Designed KHN filter output signal

The DC gain from gate-1 is $A_{Vds} = \frac{V_o}{Vi}$. The input voltage is the sum of R_6 and internal resistance from the DG MOSFET: $Vi = i(R_6 + R_{i)}$, and the output voltage is $\propto i(R_7||R_{ds1})$. Therefore, the gain is:

$$A_{Vds} = \frac{V_o}{Vi} = \frac{\propto i(R_7||R_{ds1})}{i(R_6 + R_i)} = \frac{\propto (R_7||R_{ds1})}{R_6 + R_i}$$

The input voltage is the sum of R_4 and internal resistance from the DG MOSFET: $Vi = i(R_{10} + R_i)$ and the output voltage is $\propto i(R_7||R_{ds1})$. Therefore, the gain is:

$$A_{Vds} = \frac{V_o}{Vi} = \frac{\propto i(R_7||R_{ds1})}{i(R_{10} + R_i)} = \frac{\propto (R_1||R_{ds1})}{R_{10} + R_i}$$

The software used to simulate is Multisim (v14.1). The calculations obtained the following results in Fig. 7. A capacitor equivalent replaces the resistor R_3 to capacitor C to ensure that the cut-OFF frequency is unaffected. Two equivalent capacitors are added to filter any ripple formed

from the output previous stage circuit. The following off-state circuit has been simulated. The gates of DG MOSFETs are connected to a common voltage in Fig. 7; the results are shown in Fig. 9.

Bode plotter-XBP1 shows the high-pass filter signal, bode plotter-XBP2 shows the band-pass filter signal, and bode plotter-XBP3 shows a low-pass filter signal with cut-off frequency, which is 10 kHz, but the cut-off frequency for LP is 51.078 kHz.

The magnitude gains all the signal is -6 dB, and the bandwidth is f_2-f_1 = 21.078 kHz - 4.647 kHz = 16.431 kHz. The results have been simulated and obtained results are shown in Fig. 9.

The design of the KHN biquad filter is C = 22.74 pF, R = 10 kΩ, R_1 = 15 kΩ and R_2 = 5 kΩ, R_3 =10 kΩ, and R_4 = 10 kΩ as shown in Fig. 7. The cut-off frequency is 0.7 MHz and Q = 0.7071. This analysis has been made to check these three cases. Case-I is when the two gates share the same input voltage, shown in Fig. 10. Case-II is when V_{g2} = 5 V and V_{g1} is the input signal, as shown in Fig. 11.

4.1. Case-I

The results for the proposed solution are shown in Fig. 10. The signals are displayed using the bode plotter. The cut-off frequency for the three-output signal is relatively the same, meaning the simulation was carried out well.

4.1.1. High-pass Filter Output

The output signal from the high-pass filter with a cut-off frequency of 1.0 MHz is shown in Fig. 11(a).

4.1.2. Band-pass Filter Output

The output signal from the band-pass filter with a cut-off frequency of 1.164 MHz is shown in Fig. 11(b). When the capacitance of both capacitors is large (C1 and C5=2uF), the following signal is obtained.

4.1.3. Low-pass Filter Output

The output signal from the low-pass filter with a cut-off frequency of 1.194 MHz is shown in Fig. 11(c).

4.1.4. Output Signal using AC sweep

Fig. 11(d) shows all the realized signals with their phase curves. All the cut-off frequencies for the signal are meeting closer to 45 degrees.

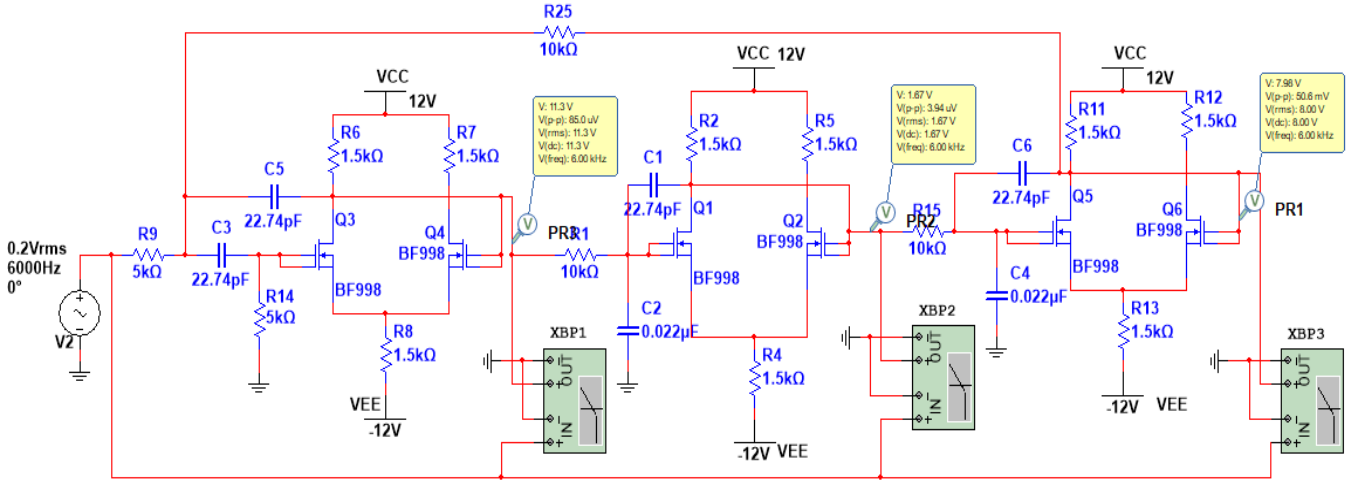

Fig. 10 CASE-1 KHN Biquad filter using DG MOSFET

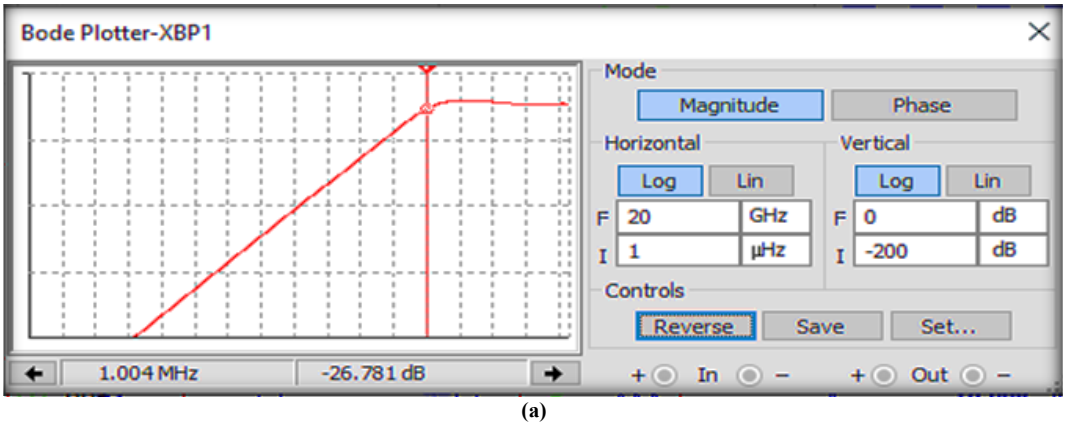

(a)

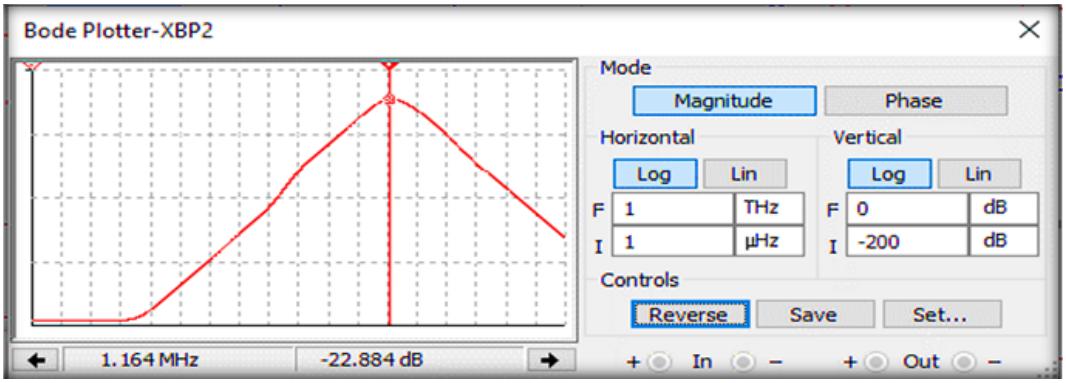

(b)

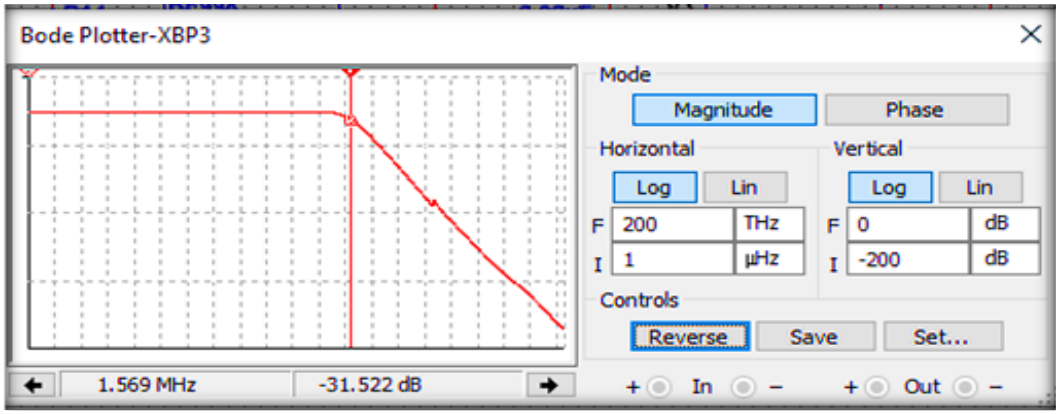

(c)

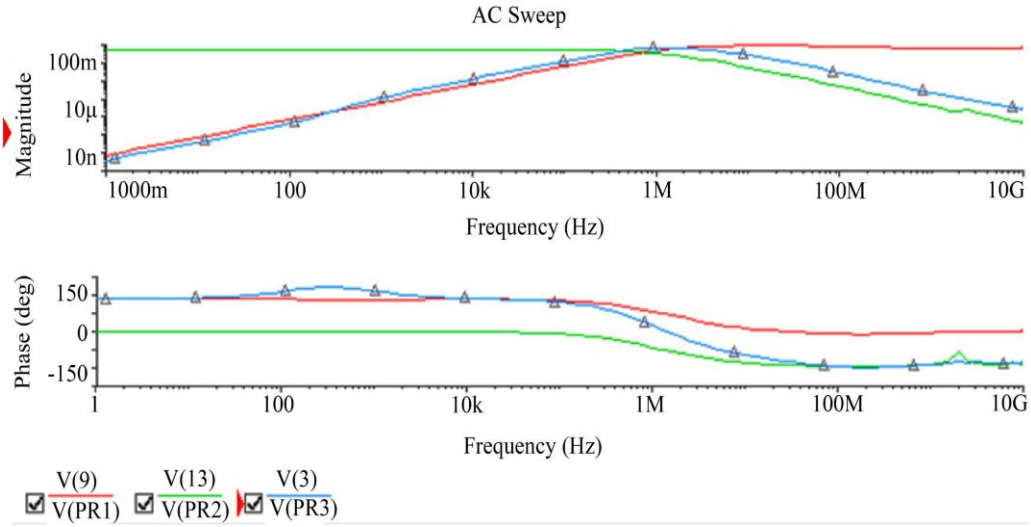

(d)

Fig. 11 (a) High-pass filter signal, (b) Band-pass filter signal when capacitance is large, (c) Low-pass filter signal, and (d) All the realized Signals

4.2. Case II

The DG MOSFET can be fed with the same input voltage signal in gate-1 and gate-2, which is the first case (Case-I) shown in Fig. 10. Now, both gates will be fed with a different input voltage signal. For this Case II, gate-2 will be fed with an AC signal, and gate-1 will be fed with 5 V DC. Hence the DG MOSFETs will be operating in the saturation region.

4.2.1. High-pass Filter Signal

The magnitude of the signal is -21.714 dB, and the cut-off frequency is around -27.479 dB. Therefore, Amax is -21.71+27.479 = 5.765 dB, which is approximately 6 dB. The straight-line part's average gradient is calculated using points A (127 kHz; -49.697 dB) and B (1.038 kHz; 91.873 dB). Therefore, the average is 0.3348 m.

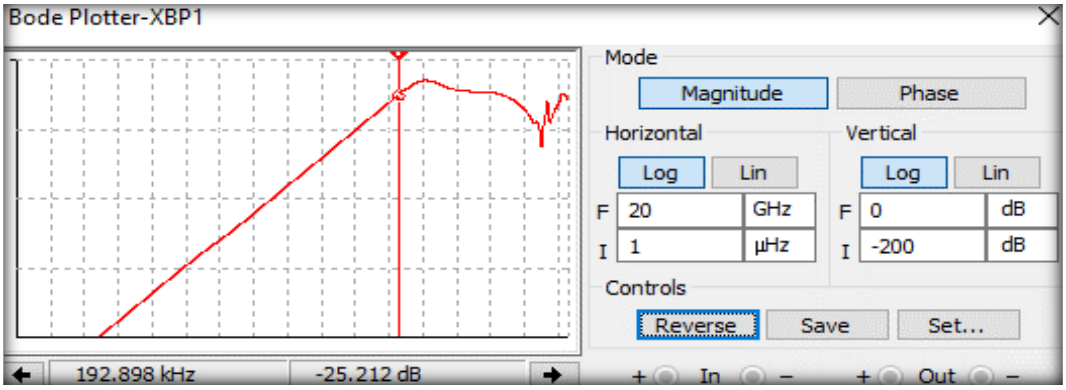

(a)

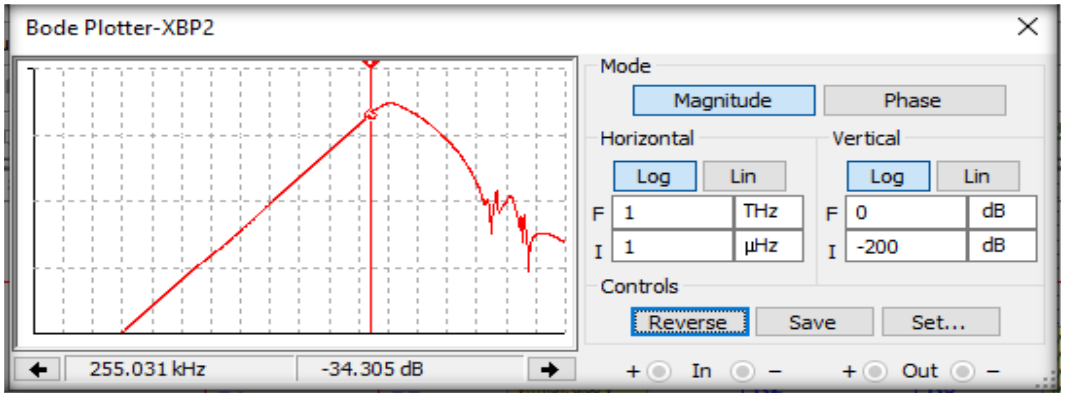

(b)

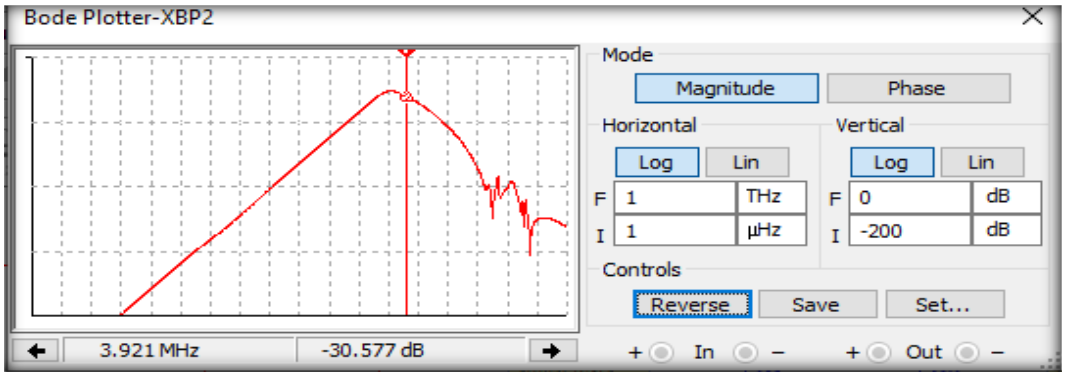

(c)

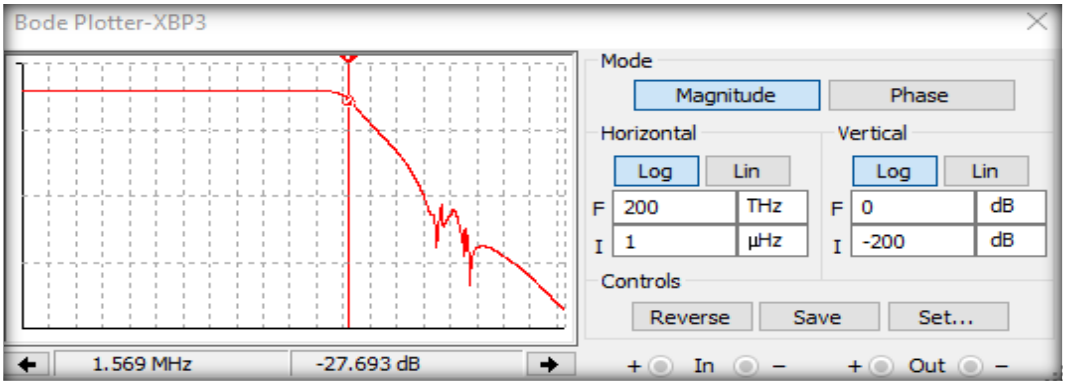

(d)

Fig. 12 (a) High-pass filter signal, (b) low-pass, (c) band-pass filter signal (at f_H), and (d) band-pass filter signal (at f_L).

4.2.2. Band-pass Filter Signal

To produce the band pass-filter, the low-pass filter and the high-pass filter are cascaded; hence, the low side of the filter will have the slope of the high-pass filter signal, and the high side will have the slope of the low-pass signal. Figure 12(b) shows the low frequency, and Fig. 12(b) shows the high frequency. The bandwidth for the band-pass signal is equivalent to the high frequency since the low frequency is way smaller than the high frequency. Therefore, the bandwidth is 3.7 MHz. The Q-factor is affected by the two capacitors, C_2 and C_4. Also, they affect the magnitude of the signal. If the capacitance of C_2 and C_4 decreases, the Q and magnitude increase. Also, the two capacitors, C2 and C4, affect the bandwidth. The magnitude of the signal is -102.685 dB, and the cut-off frequency is around -109.068 dB. Therefore A_max is -102.685+109.068 = 6.383 dB, approximately 6 dB. This shows that the system is a second-order system.

4.2.3. Low-pass Filter Signal

The datasheet specifies that the signal voltage must range from 0.1 V to 0.4 V; therefore, the suggested circuit is provided with a signal with a low voltage. The DG MOSFET's threshold voltage is 3 V. As a result; the circuit is operating in the saturation area of the triode, which is the off-state. The gates must be connected to various input voltages to reduce voltage drop. The MOSFET will start to function in the saturation area as a result.

There are some ripples in the signals which are caused by the numerous passive components in the system. The simulation proved successful, and improvements will be made to enhance the circuit and the output in light of the results.

5. Prototype Design and Analysis

The implementation of the full system has been designed as a prototype. A KHN Biquad device with the DG MOSFET has been designed to allow for isolated testing of the high-pass, low-pass, band-pass, and pass-band as individual stages. The bread-board circuit has been designed in compliance with highlighted requirements with regards to drilling sizes, track sizes, and the overall circuit size Connections have been made for the KHN filter and its associated component and equipment, according to Fig. 6 to Fig. 8 at various stages [42-45].

The input and realized signals from the three cascaded filters have been analyzed. The oscilloscope and function generator was used to test the KHN biquad filter prototype [46, 47]. The function generator's input signal (frequency) is changed to test the high-pass, band-pass, low-pass, and stop-band. Here, the frequency is varied to check if each cascade responds according to the input frequency.

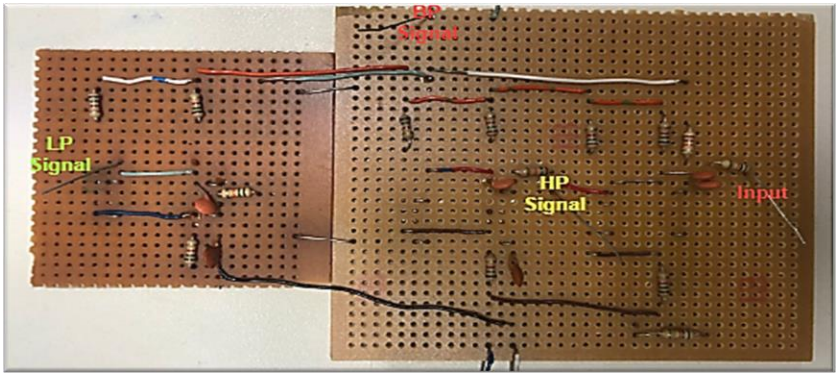

(a)

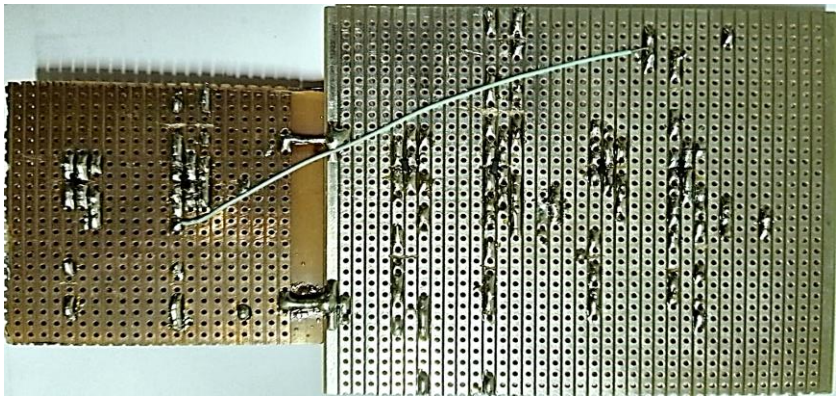

(b)

Fig. 13 KHN biquad filter prototype (a) front side and (b) backside

(a) Frequency below the cut-off frequency

(b) Frequency above the cut-off frequency

(c) Frequency below 4 kHz

(d) Frequency within the bandwidth frequency

(e) Stop-band frequency

(f) Frequency below the cut-off frequency

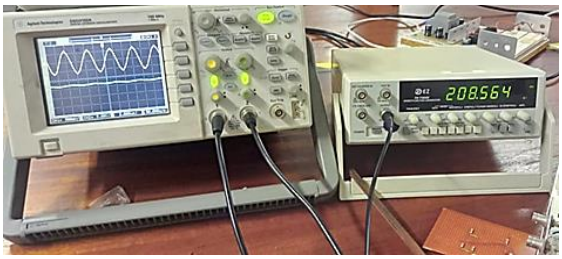

(g) Frequency above the cut-off frequency

Fig. 14 Various parametric analyses of the prototyped design

5.1. High Pass Filter

The cut-off frequency is 10 kHz for the high pass frequency. This implies that the system will reject frequencies lower than 10 kHz.When testing the system, it started responding when the input frequency was 7 kHz. Fig. 14 shows the tested results. The frequency response of the high-pass filter circuit was in-line with the simulated results.

5.2. Band-pass Filter

The cut-off frequency for the band-pass frequency is 10 kHz, while the anticipated bandwidth frequency is 41 kHz (ranges from 4 kHz to 45 kHz). This suggests that the system will reject frequencies higher than 50 kHz and lower than 4 kHz. The system responded even when the input frequency reached 50 kHz during testing but rejected frequencies greater than 35 kHz. The test results are shown in Fig. 14(e). When the frequency is within the bandwidth, the system responds by allowing the signal to pass. The results are shown in Fig. 14(d).

5.3. Low-pass Filter

The cut-off frequency for the high pass frequency is 51 kHz. This suggests that the system will reject frequencies above 51 kHz. The system began functioning when the input frequency was 60 kHz during testing. The test results are depicted in Fig. 14(g).

Compared to the op-amp-based KHN filter, the DG MOSFET-based KHN filter design performs better as the frequencies are limited in the op-amp. In addition, the DG MOSFETs are smaller and compatible, with fewer heat-up benefits, and their power consumption is lower than the op-amp based KHN filter. Therefore, the designed DG MOSFET-based KHN filter performs better.

6. Conclusion and Future Recommendations

The KHN Biquad filter prototype was fabricated and tested. Various parameters were discussed, such as the center frequency, DC gain, bandwidth, power dissipation, and quality issue. The sub-sections of this device, such as the high-pass stage filter, pass frequencies above 10 kHz; the band-pass stage filter works well for frequencies range 4 kHz - 50 kHz, and the low-pass filter allows frequencies less than 60 kHz. This work provides a Universal Biquadratic filter that dissipates less power than the original KHN biquad filter. The simulation and the circuit findings were effectively obtained by applying circuit topologies. The tested results correspond with the theoretical results. This shows that the designed prototype is in line with the expected outcome.

In the future, this device can be improved with the help of various electronic material replacements in the MOSFET, and various other improved MOSFETs (such as GAA, CSDG, FinFET, etc.) can be used.

Acknowledgment

Authors thank the University of KwaZulu-Natal, South Africa, for providing all the facilities to pursue this work.

Author Contributions

Conceptualization, ZSM; methodology, ZSM; software, ZSM; validation, ZSM and VMS; formal analysis, ZSM and VMS; investigation, ZSM and VMS; resources, ZSM; data curation, ZSM; writing—original draft preparation, ZSM; writing—review and editing, VMS; visualization, ZSM; supervision, VMS; All authors have read and agreed to the published version of the manuscript.

References

[1] Yichuang Sun, *Design of High Frequency Integrated Analogue Filters*, 1st Edition, IET, UK, 2002. [Google Scholar] [Publisher Link]

[2] R. Raut, and M. N. S. Swamy, *Modern Analog Filter Analysis and Design: A Practical Approach*, 1st Edition, Wiley, 2010. [Google Scholar] [Publisher Link]

[3] Wai-Kai Chen, *The Circuits and Filters Handbook*, 2nd Edition, CRC Press, 2003. [Google Scholar] [Publisher Link]

[4] Steve Winder, *Analog and Digital Filter Design*, 2nd Edition, Newnes, 2002. [Google Scholar] [Publisher Link]

[5] Walt Jung, *Op-Amp applications handbook*, Newnes, 2005. [Google Scholar] [Publisher Link]

[6] Muhammed A.Ibrahim, Shahram Minaei, and Hakan Kuntmana, "A 22.5 MHz Current-Mode KHN-Biquad using Differential Voltage Current Conveyor and Grounded Passive Elements," *AEU - International Journal of Electronics and Communications*, vol. 59, no. 5, pp. 311-318, 2005. [CrossRef] [Google Scholar] [Publisher Link]

[7] Costas Psychalinos, Chrysostomos Kasimis, and Fabian Khateb, "Multiple-Input Single-Output Universal Biquad Filter using Single Output Operational Transconductance Amplifiers," *AEU - International Journal of Electronics and Communications*, vol. 93, pp. 360-367, 2018. [CrossRef] [Google Scholar] [Publisher Link]

[8] S.A. Pactitis, *Active Filters: Theory and Design*, CRC Press, 2008. [Google Scholar] [Publisher Link]

[9] Chen-Nong Lee, "Independently Tunable Mixed-Mode Universal Biquad Filter with Versatile Input/Output Functions," *AEU - International Journal of Electronics and Communications*, vol. 70, no. 8, pp. 1006-1019, 2016. [CrossRef] [Google Scholar] [Publisher Link]

[10] Data R. Bhaskar, Ajishek Raj, and Pragati Kumar, "Mixed-Mode Universal Biquad Filter using OTAs," *Journal of Circuits, Systems and Computers*, vol. 29, no. 10, 2020. [CrossRef] [Google Scholar] [Publisher Link]

[11] Muhammed A. Ibrahim, Shahram Minaei, and Hakan Kuntman, "A 22.5 Mhz Current-Mode KHN-Biquad Using Differential Voltage Current Conveyor and Grounded Passive Elements," *AEU - International Journal of Electronics and Communications*, vol. 59, no. 5, pp. 311-318, 2005. [CrossRef] [Google Scholar] [Publisher Link]

[12] Danurshan Naidoo and Viranjay M. Srivastava, "Third-Order Band Pass Filter with Double-Gate MOSFET: A Circuit Perspective," *11th International Conference on Computer Communication and Informatics*, pp. 1-6, 2021. [CrossRef] [Google Scholar] [Publisher Link]

[13] Jetsdaporn Satansup, Tattaya Pukkalanun, and Worapong Tangsrirat, "Current-Mode KHN Biquad Filter using Modified CFTAs and Grounded Capacitors," *International MultiConference of Engineers and Computer Scientists*, 2011. [Google Scholar] [Publisher Link]

[14] San Fu Wang et al., "Voltage-Mode Multifunction Biquad Filter and its Application as Fully-Uncoupled Quadrature Oscillator Based on Current-Feedback Operational Amplifiers," *Sensors*, vol. 20, no. 22, p. 6681, 2020. [CrossRef] [Google Scholar] [Publisher Link]

[15] Viranjay M. Srivastava, K. S. Yadav, and G. Singh, "Explicit Model of Cylindrical Surrounding Double-Gate MOSFETs," *WSEAS Transactions on Circuits and Systems*, vol. 12, no. 3, pp. 81-90, 2013. [Google Scholar] [Publisher Link]

[16] M. Sagbas, and M. Koksal, "A New Multi-Mode Multifunction Filter Using CDBA," *European Conference on Circuit Theory and Design*, Cork, Ireland, vol. 2, pp. 225-228, 2005. [CrossRef] [Google Scholar] [Publisher Link]

[17] A. Tugberk Bekri, and F. Anday, "Nth-Order Low-Pass Filter Employing Current Differencing Transconductance Amplifiers," *European Conference on Circuit Theory and Design*, Cork, Ireland, pp. 193-196, 2005. [CrossRef] [Google Scholar] [Publisher Link]

[18] Sinem Olmez, and Ugur Cam, "A Novel Square Root Domain Lossless Integrator and its Application to KHN Biquad Filter Design," *International Conference on Electrical and Electronics Engineering*, Bursa, Turkey, pp. 227-230, 2009. [CrossRef] [Google Scholar] [Publisher Link]

[19] Hamed Aminzadeh, and Dalton Martini Colombo, "Analysis and Design Procedures of CMOS OTAs Based on Settling Time," *Journal of Integrated Circuits and Systems*, vol. 17, no. 1, 2022. [CrossRef] [Google Scholar] [Publisher Link]

[20] Esraa M. Hamed et al., "Effect of Different Approximation Techniques on Fractional-Order KHN Filter Design," *Circuits, Systems, and Signal Processing*, vol. 37, pp. 5222–5252, 2018. [CrossRef] [Google Scholar] [Publisher Link]

[21] T. S. Rathore, and Prasoon Vishwakarma, "Realizations of Conventional and Inverse Voltage Transfer Functions," *SSRG International Journal of Electronics and Communication Engineering*, vol. 8, no. 9, pp. 1-4, 2021. [CrossRef] [Publisher Link]

[22] Ramakant A. Gayakwad, *Op-Amps and Linear Integrated Circuits*, Prentice Hall, 2003. [Google Scholar] [Publisher Link]

[23] Adel S. Sedra, and Kenneth C. Smith, *Microelectronic Circuits: Theory and Applications*, 7th Edition, Oxford University Press, USA, 2014. [Google Scholar]

[24] Viranjay M. Srivastava, and Ghanshyam Singh, "MOSFET Technologies for Double-Pole Four Throw Radio Frequency Switch," *Analog Circuits and Signal Processing*, Switzerland, vol. 122, 2014. [CrossRef] [Google Scholar] [Publisher Link]

[25] BF998, BF998R Silicon N-Channel Dual Gate MOSFET Datasheet, NXP Semiconductors, 1996. [Publisher Link]

[26] BF909, BF909R N-Channel Dual Gate MOS-FETs Data Sheet, 2007. [Publisher Link]

[27] P. M. Solomon et al., "Two Gates are Better than One [Double-Gate MOSFET Process]," *IEEE Circuits and Devices Magazine*, vol. 19, no. 1, pp. 48–62, 2003. [CrossRef] [Google Scholar] [Publisher Link]

[28] Yuan Taur, and Huang H. Lin, "Modeling of DG MOSFET I–V Characteristics in the Saturation Region," *IEEE Transactions on Electron Devices*, vol. 65, no. 5, pp. 1714-1720, 2018. [CrossRef] [Google Scholar] [Publisher Link]

[29] Douglas A. Pucknell, *Basic VLSI Design*, Prentice Hall, 1994. [Google Scholar]

[30] Revna A. Vural et al., "CMOS Differential Amplifier Area Optimization with Evolutionary Algorithms," *Proceedings of the World Congress on Engineering and Computer Science*, San Francisco, CA, USA, 2013. [Google Scholar] [Publisher Link]

[31] H. H. Afshari, S. A. Gadsden, and S. Habibi, "Gaussian Filters for Parameter and State Estimation: A General Review of Theory and Recent Trends," *Signal Processing*, vol. 135, pp. 218-238, 2017. [CrossRef] [Google Scholar] [Publisher Link]

[32] Tajinder Singh Arora, and R. K. Sharma, "An All-Mode KHN Equivalent Biquad using Third Generation Current Conveyor and All Grounded Passive Elements," *Proceedings of the National Academy of Sciences, India, Section A: Physical Sciences*, vol. 87, pp. 97-108, 2017. [CrossRef] [Google Scholar] [Publisher Link]

[33] Behzad Razavi, "The Biquadratic Filter [A Circuit for All Seasons]," *IEEE Solid-State Circuits Magazine*, vol. 10, no. 2, pp. 11– 109, 2018. [CrossRef] [Google Scholar] [Publisher Link]

[34] Electronic Tutorial, State Variable Filter. [Online]. Available: https://www.electronics-tutorials.ws/filter/state-variable-filter.html

[35] Jared Wuerzburger, and Oscar G. Henriquez, "Multimedia Learning: Simulated vs. Real-World Digital Logic Circuit Curriculum," *IGI Global*, 2019. [CrossRef] [Google Scholar] [Publisher Link]

[36] Suvashan Pillay and Viranjay M. Srivastava, "Design and Comparative Analysis of Active-Loaded Differential Amplifier using Double-Gate MOSFET," *SN Applied Science*, vol. 4, no. 8, 2022. [CrossRef] [Google Scholar] [Publisher Link]

[37] Dylan Pillay, and Viranjay M. Srivastava, "Realization with Fabrication of Dual-Gate MOSFET based Source Follower," *Silicon*, vol. 14, no. 17, pp. 11979-11989, 2022. [CrossRef] [Google Scholar] [Publisher Link]

[38] Keita Tachiki et al., "Short-Channel Effects in Sic MOSFETs based on Analyses of Saturation Drain Current," *IEEE Transactions on Electron Devices*, vol. 68, no. 3, pp. 1382 – 1384, 2021. [CrossRef] [Google Scholar] [Publisher Link]

[39] Nikolaos Makris et al., "Charge-Based Modeling of Long-Channel Symmetric Double-Gate Junction FETs—Part I: Drain Current and Transconductances," *IEEE Transactions on Electron Devices*, vol. 65, no. 7, pp. 2744-2750, 2018. [CrossRef] [Google Scholar] [Publisher Link]

[40] Naveenbalaji Gowthaman, and Viranjay M. Srivastava, "Capacitive Modeling of Cylindrical Surrounding Double-Gate MOSFETs for Hybrid RF Applications," *IEEE Access*, vol. 9, pp. 89234-89242, 2021. [CrossRef] [Google Scholar] [Publisher Link]

[41] Luis Abraham Sánchez-Gaspariano et al., "CMOS Analog Filter Design for Very High Frequency Applications," *Electronics*, vol. 9, no. 2, p. 362, 2020. [CrossRef] [Google Scholar] [Publisher Link]

[42] Naveenbalaji Gowthaman, and Viranjay M. Srivastava, "Mathematical Modeling of Drain Current Estimation in a CSDG MOSFET, Based on La_2O_3 Oxide Layer with Fabrication—A Nanomaterial Approach," *Nanomaterials*, vol. 12, no. 19, p. 3374, 2022. [CrossRef] [Google Scholar] [Publisher Link]

[43] Ling Lu, "Topology on a Bread-Board," *Nature Physics*, vol. 14, 875–877, 2018. [CrossRef] [Google Scholar] [Publisher Link]

[44] Naveenbalaji Gowthaman, and Viranjay M. Srivastava, "Design of Cylindrical Surrounding Double-Gate MOSFET with Fabrication Steps using a Layer-by-Layer Approach," *IEEE Access*, vol. 10, pp. 116059 - 116068, 2022. [CrossRef] [Google Scholar] [Publisher Link]

[45] Paul R. Gray et al., *Analysis and Design of Analog Integrated Circuits*, 5th Edition, Wiley, 2009. [Google Scholar] [Publisher Link]

[46] Eric Macdonald et al., "3D Printing for the Rapid Prototyping of Structural Electronics," *IEEE Access*, vol. 2, pp. 234-242, 2014. [CrossRef] [Google Scholar] [Publisher Link]

[47] R. S. Khandpur, *Printed Circuit Boards: Design, Fabrication, Assembly and Testing*, Tata McGraw-Hill Education, 2005. [Google Scholar] [Publisher Link]

[48] From Moore's Law to NTRS to ITRS to IRDS, International Roadmap for Devices and Systems, 2020. [Publisher Link]